Article

Journal of the Brazilian Chemical Society

https://dx.doi.org/10.21577/0103-5053.20230180

J. Braz. Chem. Soc. **2024**, *35*, 5, e-20230180, 1-14

Experimental Design Modelling and Optimization of the Intercalation of Levofloxacin and Salicylic Acid into the Structure of ZnAl-LDH by Response Surface Method: *in vitro* Study of Release Kinetics, Antibacterial and Anti-Inflammatory Activities

Ngo T. T. Vy,[a,b] Dang N. N. Khanh,[a] Le H. Khoa,[a,c] Nguyen T. Phat,[d] Nguyen Q. Thang,[e] Le H. Trung,[e] Nguyen T. H. Nhu,[e] Doan T. M. Phuong[f] and Nguyen T. K. Phuong[*,a,b]

[a]Graduate University of Science and Technology, Vietnam Academy of Science and Technology, Hanoi 100000, Vietnam

[b]Institute of Applied Materials Science, Vietnam Academy of Science and Technology, Ho Chi Minh 700000, Vietnam

[c]Institute for Tropical Technology, Vietnam Academy of Science and Technology, Hanoi 100000, Vietnam

[d]Institute of Chemical Technology, Vietnam Academy of Science and Technology, Ho Chi Minh 700000, Vietnam

[e]Faculty of Chemical Engineering, Industrial University of Ho Chi Minh City, Ho Chi Minh 700000, Vietnam

[f]Faculty of Chemical Engineering, Ho Chi Minh City University of Industry and Trade, Ho Chi Minh 700000, Vietnam

In recent years, solid-state engineering has emerged as a promising method for improving the stability and potency of antibiotics and anti-inflammatory drugs. This study focuses on the design and optimization of the intercalation of levofloxacin (an antibiotic drug) and salicylic acid (an anti-inflammatory drug) into zinc-aluminium-layered double hydroxide galleries using response surface method. Release studies revealed that a burst release phenomenon was observed at the beginning of the release assay, and the pH value (in the range of 5.8-7.4) had very little influence on the levofloxacin and salicylic acid release efficiency. This indicates that zinc-aluminium-layered double hydroxide could be an effective inorganic carrier for levofloxacin and salicylic acid over a wide range of pH values. Four kinetic models were used to study the release kinetics and the drug release mechanism was also discussed. In addition, the intercalation of levofloxacin and salicylic acid into zinc-aluminium-layered double hydroxide exhibited enhanced antibacterial activity against Gram-positive *Bacillus subtilis*. The cell viability assay revealed non-toxic behavior of levofloxacin and salicylic acid intercalated into zinc-aluminium-layered double hydroxide against the monocyte/macrophage-like cell line.

Keywords: experimental design, optimization, response surface methodology, zinc-aluminium-layered double hydroxide, levofloxacin, salicylic acid

Introduction

In recent years, drug delivery systems that deliver therapeutic agents to their target sites have attracted significant attention. Nanoparticle-based drug delivery technologies have advanced from the need to optimize and maintain therapeutic drug concentrations for a sufficiently long time, minimize negative side effects, control drug release, deliver drugs to target tissues, enhance the effects of drugs with short half-lives, reduce dosing frequency, and avoid drug waste.[1] Layered double hydroxides (LDHs) with two-dimensional layered nanostructures are emerging as promising materials that have launched a new field of research to investigate their use as drug delivery systems. Recent *in vitro* studies[2,3] using a range of transformed and tumor-derived cell lines indicate that LDHs nanoparticles have low cytotoxicity and good biocompatibility. Positively charged LDHs nanoparticles can readily interact with negatively charged cell membranes and rapidly enter cells via the clathrin-mediated intracellular pathway, which is the most common energy-dependent endocytic pathway.[4,5] LDHs are guest-host materials consisting of positively charged metal hydroxide sheets

*e-mail: nguyenthikimp@yahoo.ca
Editor handled this article: Ivo M. Raimundo Jr. (Associate)

as hosts, intercalated anions as guests, and water molecules. The general chemical formula of an LDH is $[M(II)_{1-x}M(III)_x \cdot (OH)_2]^{x+} \cdot [A^{n-}]_{x/n} \cdot mH_2O$. The positively charged layers contain divalent(II) and trivalent(III) metal (M) ions, and the interlayer region is occupied by charge-balancing anions. The A^{n-} anions, such as CO_3^{2-}, NO_3^-, and Cl^-, in the interlayer galleries can be readily replaced;[6] thus, anionic drugs can be conveniently loaded into LDHs via anion exchange.[2,7] The most fascinating feature of LDHs is that they have very large specific surface areas; therefore, high drug loading is possible into the interlayer regions of LDHs. As another bonus, LDHs at the nanoscale are easily dispersible in aqueous media.

Many biomolecular anions, including pravastatin, fluvastatin,[8] ibuprofen, paracetamol, diclofenac,[9-11] naproxen,[12] ciprofloxacin,[13] methotrexate, 5-fluorouracil[14-17] and DL-mandelic acid[18] have been successfully intercalated into the interlayers of LDHs. However, these studies on LDHs drug delivery systems have mainly involved oral drug simulation experiments. LDHs are also used as drug delivery systems for wounds and have rarely been considered in this context. Additional materials such as zinc may be added to an LDHs to enhance its biocompatibility. Because of its ionic form, zinc plays a vital role in the human body, where it protects against deoxyribonucleic acid (DNA) damage, is useful in cancer therapy, and controls the activities of many enzymes.[19-24] To date, zinc-aluminium-layered double hydroxide (ZnAl-LDH) has been used for the delivery of many drugs, including antibiotic, anti-inflammatory, cholesterol-lowering,[25] and anticancer.[26,27] ZnAl-LDH is an ideal delivery system for wound treatment owing to its low toxicity and good biocompatibility. The effectiveness and side effects of such delivery systems for antibiotic and anti-inflammatory drugs, as well as target cells in the wound, have yet to be explored. In addition, it is recommended to optimize the influencing factors on the intercalation of antibiotic and anti-inflammatory drugs into such delivery systems. However, optimization by factor-by-factor approach is more time consuming and not economically efficient. Therefore, statistical experimental designs, particularly the response surface method (RSM), excellent optimization tools, have been developed to solve this problem. The RSM, including factor design and regression analysis, can give clear knowledge of the perfect and efficient relationship between independent and dependent variables to achieve desired results. The great advantage of RSM is to reduce testing time and effort, achieves better results, and saves more costs compared to traditional experimental models.

In continuation to our previous studies on biocompatible ZnAl-LDH materials,[28] with emphasis on the effective delivery of therapeutic drugs to a wound at the right dose and time, this study focuses on experimental design to optimize the intercalation of antibiotic (levofloxacin-LEV) and anti-inflammatory (salicylic acid-SAL) into the ZnAl-LDH structure. An attempt was made to intercalate drugs (LEV and SAL) into ZnAL-LDH using the face centered-central composite design (FC-CCD). To do this, 3 levels of +1, 0, −1 and three independent variables (factors), i.e., temperature, time and initial drug amount were selected. The formulation of drugs was studied for characterization, bioactivity, and release kinetics. These findings may provide valuable information in the fields of chemistry and pharmaceuticals to promote solid-state materials as an antibiotic development strategy.

Experimental

This study used chemicals that were purchased from Sigma-Aldrich (St. Louis, Missouri, USA) and are presented in the Supplementary Information (SI) section.

Optimization of drug intercalated into ZnAl-LDH using a face centered-central composite design (FC-CCD)

The synthesis of ZnAl-LDH was performed according to our previous study[28] and is presented in the SI section.

Statistical design for drug intercalated into the structure of ZnAl-LDH

FC-CCD was used to optimize drug intercalation into ZnAl-LDH. Three independent variables were selected: temperature (X_1), time (X_2), and amount of drug (LEV or SAL) (X_3). Each factor was tested at three levels, which were coded as −1, 0, and +1. The design levels, independent factors, and change ranges are listed in Table 1.

Table 1. Independent variables, experimental range, and levels for FC-CCD (the amount of ZnAl-LDH kept constant at 1.0 g in all experiments)

Coded values	Variable and range		
	Temperature (X_1) / °C	time (X_2) / h	Amount of drug (X_3) / g
High (+1)	75.0	19.0	1.00
Medium (0)	65.0	17.5	0.75
Low (–1)	55.0	16.0	0.50

The response (Y) was the dependent variable expressing the efficiency of the drug intercalation into ZnAl-LDH. Responses were analyzed using MODDE 5.0 software (Umetrics AB, Umea, Sweden)[29] and Design-Expert

software (version 13.0.5.0; Stat-Ease Inc., MN, USA).[30] The model was statistically significant if the probability value (*p*-value) was less than 0.05 (95% confidence level).

RSM graphs were used to evaluate the observed data systematically and establish quadratic polynomial equations. The quadratic polynomial equation, which indicates the interactions between variables and the relationships between responses and variables, is expressed as follows:

$$Y = \sum_{i=1}^{3} b_i X_i + \sum_{i=1}^{3} b_{ii} X_i^2 + \sum_{i \neq j,\ i=1,\ j=2}^{3} b_{ij} X_i X_j + b_0 \quad (1)$$

where, Y is the predict dependent variable; X_i and X_i^2 are the independent variables and quadratic parameters, respectively; X_iX_j represents the interaction of independent variable b_0, and b_i, b_{ii}, b_{ij} represent the regression coefficient for intercept and corresponding regression coefficients, respectively.

Drug intercalation into ZnAl-LDH was conducted under an N_2 atmosphere and sonicated at 100 W in an ultrasonic bath. ZnAl-LDH (1.0 g) was dispersed in 250 mL of a solution containing LEV or SAL at a concentration ranging from 0.5 to 1.0 g. The reaction mixture was heated to 55-75 °C for 16-19 h. The solid products were obtained through filtration, washing with decarbonized distilled water, and drying for 18 h at 70 °C. The quantification of the percentage of LEV or SAL intercalated into ZnAl-LDH was performed by measuring the total organic carbon (TOC) concentration in LEV-LDH and SAL-LDH samples. The calculations involved comparing the TOC values with the formulas for pure levofloxacin ($C_{18}H_{20}FN_3O_4$) and salicylic acid ($C_7H_6O_3$). The TOC concentration was measured using CHNSO elemental analysis (Mettler Toledo, USA). The percentage of the drug intercalated into ZnAl-LDH was determined as follows:

$$\text{Drug intercalated}(\%) = \frac{TOC_{drug-LDH} - TOC_{ZnAl-LDH}}{TOC_{initial\ solution}} \times 100 \quad (2)$$

where $TOC_{drug\text{-}LDH}$: concentration of organic carbon in sample drug-LDH; $TOC_{ZnAl\text{-}LDH}$: concentration of organic carbon in ZnAl-LDH; $TOC_{initial\ solution:}$ concentration of organic carbon in solution.

Validation of experimental design

By using optimized temperature, time and drug dosage, drug-LDH samples were fabricated and evaluated for various parameters including composition and characterization of drug-LDH samples, and *in vitro* studies (i.e., release kinetics, antimicrobial and cytotoxic assays). Validation of the experimental design was performed through the calculation of the relative error using the following formula:

$$\text{Relative error}(\%) = \frac{\text{Predicted values} - \text{Observed values}}{\text{Predicted values}} \times 100 \quad (3)$$

Characterization and *in vitro* studies of drug-LDH

Characterization, inorganic elements (Zn, Al, F), organic elements (C, H, N, O) and *in vitro* studies of drug-LDH including drugs release kinetics, antimicrobial activity and cytotoxicity assays are presented in the SI section.

Results and Discussion

Optimization of drug intercalated into ZnAl-LDH

Influence of the independent variables on drug intercalated into ZnAl-LDH

In this study, a FC-CCD experimental design with three levels and three independent variables was used to investigate the combined effects of the three independent variables on the interactions of LEV or SAL and ZnAL-LDH. The experimental parameters and corresponding results are listed in Table 2.

Furthermore, the significant regression coefficients of the quadratic equations and the results of the analysis of variance (ANOVA) were summarized in Table 3.

The quadratic equations 4 and 5 were expressed as follows:

$$Y_{LEV-LDH} = 2.25X_1 + 1.40X_2 + 1.89X_3 - 3.06X_1^2 - 1.30X_2^2 - 1.27X_3^2 + 1.20X_1X_3 + 34.79 \quad (4)$$

$$Y_{SAL-LDH} = 2.40X_1 + 1.32X_2 + 1.76X_3 - 3.31X_1^2 - 1.42X_2^2 + 0.85X_1X_3 + 47.42 \quad (5)$$

For LEV-LDH, *p* values for linear variables (X_1, X_2, X_3), 2-way interaction (X_1X_3), and quadratic parameters (X_1^2, X_2^2, X_3^2) were all < 0.05, which significantly influenced the loading of LEV on ZnAl-LDH. In contrast, X_1X_2 and X_2X_3 were not significantly affected by the loading effect ($p > 0.05$). As expressed in equation 4, the effect of temperature (X_1) on the loading of LEV on ZnAl-LDH was the greatest among the three linear variables with a coefficient of 2.25, followed by the effect of the amount of LEV (X_3) with a coefficient of 1.88. The quadratic equation 4 exhibited a positive effect of temperature (X_1), time (X_2), and amount of LEV (X_3) on the loading of LEV onto ZnAl-LDH. For the effect of the quadratic parameters (X_1^2, X_2^2, and X_3^2) on the loading of LEV on ZnAl-LDH,

Table 2. Response data for FC-CCD-designed experimental runs for LEV and SAL intercalated into ZnAl-LDH

No.	Variable levels			LEV-LDH			SAL-LDH		
				Observed		Predicted LEV intercalated / %	Observed		Predicted SAL intercalated / %
	Temp. (X_1)	time (X_2)	Amount of drug (X_3)	TOC / mg	LEV intercalated / %		TOC / mg	SAL intercalated / %	
1	−1	−1	−1	0.145	24.22	24.23	0.218	35.82	36.51
2	1	−1	−1	0.165	27.50	27.10	0.245	40.23	40.36
3	−1	1	−1	0.172	28.80	28.23	0.247	40.57	40.40
4	1	1	−1	0.175	29.24	29.56	0.260	42.74	42.74
5	−1	−1	1	0.158	26.40	26.04	0.236	38.76	38.82
6	1	−1	1	0.199	33.19	33.72	0.279	45.86	46.09
7	−1	1	1	0.172	28.80	29.16	0.254	41.77	41.70
8	1	1	1	0.211	35.35	35.31	0.293	48.08	47.45
9	−1	0	0	0.173	28.92	29.48	0.257	42.22	41.71
10	1	0	0	0.206	34.40	33.99	0.281	46.24	46.51
11	0	−1	0	0.191	31.88	32.09	0.279	45.79	44.69
12	0	1	0	0.209	34.96	34.89	0.283	46.45	47.32
13	0	0	−1	0.185	31.00	31.63	0.276	45.38	44.73
14	0	0	1	0.215	35.90	35.41	0.291	47.83	48.24
15	0	0	0	0.210	35.10	34.79	0.286	47.03	47.42
16	0	0	0	0.209	34.95	34.79	0.286	46.94	47.42
17	0	0	0	0.207	34.60	34.79	0.291	47.82	47.42

Temp: temperature; TOC: total organic carbon; LEV: levofloxacin; SAL: salicylic acid; LEV-LDH: levofloxacin intercalated into layered double hydroxide; SAL-LDH: salicylic acid intercalated into layered double hydroxide.

Table 3. ANOVA for quadratic equations of LEV and SAL intercalated into ZnAl-LDH

Source of variation	LEV intercalated				SAL intercalated			
	Mean squares	Degrees of freedom	*F*-value	*p*-value	Mean squares	Degrees of freedom	*F*-value	*p*-value
Regression	23.46	9	66.58	< 0.0001	23.21	9	36.84	< 0.0001
X_1	50.78	1	114.12	< 0.0001	57.65	1	91.51	< 0.0001
X_2	19.50	1	55.35	0.0001	17.29	1	27.45	0.0012
X_3	35.65	1	101.17	< 0.0001	30.84	1	48.95	0.0002
X_1^2	25.02	1	70.99	< 0.0001	29.34	1	46.57	0.0002
X_2^2	5.40	1	12.78	0.0090	5.40	1	8.57	0.0221
X_3^2	4.29	1	12.18	0.0101	2.34	1	3.71	0.0954
X_1X_2	1.19	1	3.37	0.1091	1.15	1	1.82	0.2191
X_1X_3	11.57	1	32.83	0.0007	5.83	1	9.26	0.0188
X_2X_3	0.39	1	1.10	0.3295	0.52	1	0.82	0.3959
Residual	0.35	7	–	–	0.63	7	–	–
Lack of fit	0.4670	5	7.09	0.1282	0.7882	5	3.36	0.2450
Pure error	0.0658	2	–	–	0.2344	2	–	–
Total corrected	13.35	16	–	–	13.33	16	–	–
	RSD = 0.5936 R^2 = 0.9885		Predicted R^2 = 0.8496 Adjusted R^2 = 0.9736		RSD = 0.7937 R^2 = 0.9793		Predicted R^2 = 0.8302 Adjusted R^2 = 0.9527	

LEV: levofloxacin; SAL: salicylic acid; *p*-value: probability value; *F*-value: value of variation between sample means; RSD: relative standard deviation; R^2: coefficient of determination; X_1: temperature; X_2: time; X_3: amount of drug.

the coefficient value of the quadratic parameter X_1^2 was −3.06 (equation 4), the greatest negative effect among the three quadratic parameters. For the 2-way interaction, X_1X_3 had a positive effect on the loading of LEV on ZnAl-LDH, with a coefficient of 1.20.

For SAL-LDH, linear variables (X_1, X_2, X_3), 2-way interaction (X_1X_3) and quadratic parameters (X_1^2, X_2^2), significantly impacted the loading of SAL on ZnAl-LDH ($p < 0.05$). X_3^2, X_1X_2, and X_2X_3 exhibited no significant loading effects ($p > 0.05$). Of the three linear variables, temperature (X_1) had the greatest positive effect on the loading of SAL onto ZnAl-LDH, with a coefficient of +2.40, whereas time (X_2) had the lowest positive effect, with a factor value of +1.32. For the 2-way interaction, X_1X_3 had a slightly positive effect on the loading of SAL onto ZnAl-LDH with a coefficient of +0.85. As expressed in equation 5, the quadratic parameters X_1^2 and X_2^2 had a negative effect on the loading of LEV onto ZnAl-LDH. The quadratic parameter X_1^2 had a more significant effect than X_2^2.

The importance of temperature (X_1) in the intercalation of LEV and SAL into ZnAl-LDH could be explained by the diffusion phenomenon. Diffusion was the movement of atoms or molecules from an area of high concentration to a region of low concentration. The kinetic energy of matter increased at high temperature, leading to an increase in the diffusion of drug molecules into the interlayer region of ZnAl-LDH. The movement of drug molecules decreased at low temperatures, leading to a decrease in diffusion of drug molecules into the interlayer region of ZnAl-LDH.

The ANOVA results of the quadratic equations indicated high significance of the model (Table 3). To confirm the best fit of the model, statistical parameters such as *p*-value, lack of fit, coefficient of determination (R^2), relative standard deviation (RSD), adjusted R^2, and predicted R^2 were used. The *p*-value was small ($p < 0.05$), indicating high significance of the corresponding coefficients. The *p*-value was very low ($p < 0.0001$), indicating statistical significance of the regression model at the 95% confidence level.

Similarly, the ANOVA results demonstrated that the *p*-value of the lack-of-fit for LEV and SAL were 0.128 and 0.245, respectively, which are significantly higher than 0.05. This shows that, because of the random error of the experimental variations, the lack of fit was insignificant, and the regression models for LEV and SAL well adjusted. In addition, the relatively low RSD value (0.5936-0.7937) indicates that the use of RSM was reliable and the model precision was good. The R^2 (goodness of fit) and adjusted R^2 values of the LEV and SAL regression models are approximately equal and close to 1.0, indicating that the regression model fits the observed data. The prediction level of the model was also satisfactory; the predicted R^2 value (goodness of prediction) for both regression models was greater than 0.80. This indicates that the RSM of the observed data was accurate.

The obtained quadratic regression equations helped establish three-dimensional response surface plots (3D-RSPs) based on the optimized conditions of temperature, time, and drug quantity. These 3D-RSPs elucidated the influence of the 2-way interactions on the incorporation of LEV and SAL into ZnAl-LDH, and the results are shown in Figure 1.

For LEV-LDH (Figures 1a-1c), temperature had the greatest effect on the efficiency of LEV intercalation into ZnAl-LDH, whereas the effects of time and amount of LEV on the efficiency of LEV intercalation into ZnAl-LDH were the same, and both factors had less influence than temperature. For SAL-LDH (Figures 1d-1f), temperature had the greatest influence on the efficiency of LEV intercalation into ZnAl-LDH, followed by the amount of SAL and final time.

Validation of experimental design

Based on the analysis of the intercalation efficiency and the response surface plots illustrated in Figure 1, the optimal conditions for intercalation of LEV and SAL into ZnAl-LDH were determined as a temperature level of 70 °C, reaction time of 18 h, and drug quantity of 1.0 g. By implementing the optimal conditions determined, LEV-LDH and SAL-LDH samples were prepared to validate the experimental design and facilitate further studies. The results of these experiments are listed in Table 4.

The experimental design was validated by comparing observed and predicted values. The relative errors associated with the observed and predicted values were determined to be within an acceptable range of ± 5% (Table 4). The predicted results closely matched the experimental results, confirming the accuracy of the design.

Characterization of the materials

Based on results of elemental analysis (Table 5) and the charge balance principle, the empirical formulas of LEV-LDH and SAL-LDH are predicted to be $Zn_{1.44}Al_{0.42}(OH)_4(C_{18}H_{20}FN_3O_4)_{0.26}$ and $Zn_{1.38}Al_{0.42}(OH)_3(C_7H_6O_3)$, respectively. The results in parentheses presented in Table 5 calculated from the predicted formulas agree very well with the observed data, which confirms that the predicted chemical formula is appropriate.

Thermal analysis was carried out to confirm the efficiency of intercalation of drug into ZnAl-LDH. Our

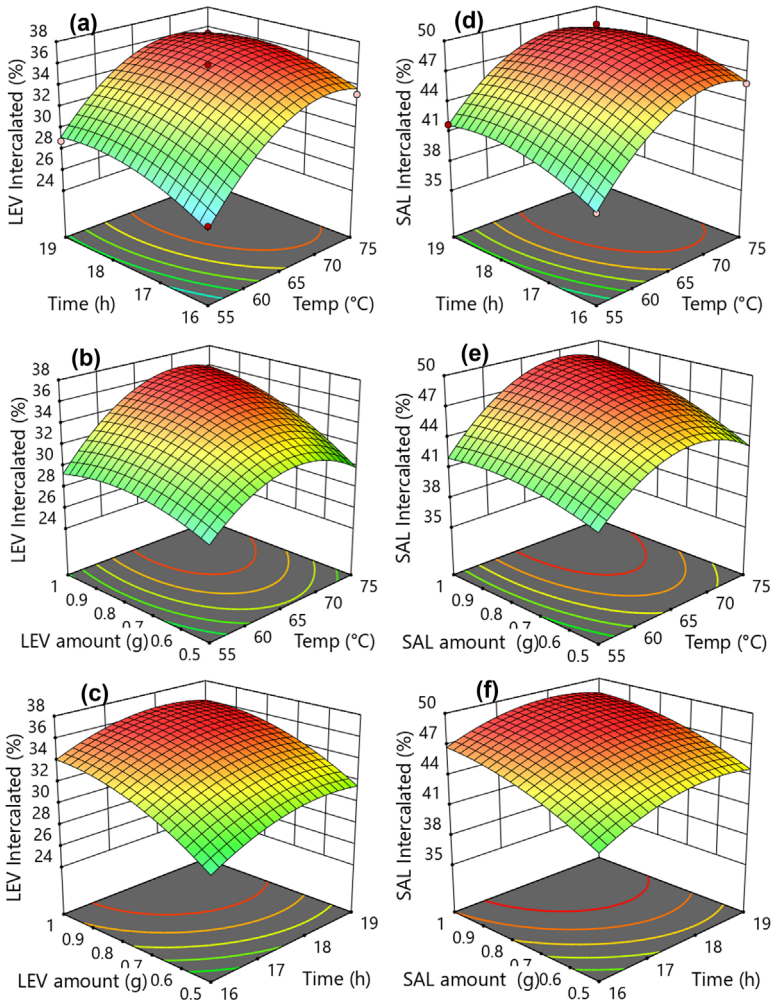

Figure 1. Response surface plots of LEV (a-c) and SAL (d-f) intercalated into ZnAl-LDH structure at optimum condition.

Table 4. Drugs intercalated into ZnAl-LDH (predicted value obtained from quadratic equations using optimized conditions)

Drug	Predicted value / %	Observed value / %	Relative error / %
LEV	36.56	35.35	3.34
SAL	49.18	48.00	2.40

LEV: levofloxacin; SAL: salicylic acid.

previous publication[28] has shown that ZnAl-LDH material has three weight losses of about 8.0% at temperatures between 116 and 455 °C and one weight loss of about 2.1% at a temperature of 620 °C. The weight losses at temperature from 116 to 455 °C were indexed for the removal of surface-physiosorbed water molecules and the interlayer water in the ZnAl-LDH structure. The weight loss at 620 °C was attributed to the further degradation of the inorganic layer

Table 5. Chemical composition of the LEV-LDH and SAL-LDH

Sample	Element[a] / %						
	Zinc (Zn)	Aluminium (Al)	Oxygen (O)	Organic carbon (C)	Nitrogen (N)	Hydrogen (H)	Fluor (F)
LEV-LDH	34.76 (34.76)	4.24 (4.24)	30.83 (29.95)	21.15 (21.15)	4.11 (4.20)	3.45 (3.44)	1.86 (1.86)
SAL-LDH	31.48 (31.48)	3.92 (3.92)	32.32 (33.40)	29.21 (29.21)	–	3.10 (3.13)	–

[a]Observed data (the data are computed from the proposed empirical formulas) using ICP-OES (PerkinElmer, USA) to analyze Zn and Al; ion chromatography (IC) (Metrohm, Switzerland) to analyze F and CHNSO elemental analysis (Mettler Toledo, USA) to analyze C, H, O and N. LEV-LDH: levofloxacin intercalated into layered double hydroxide; SAL-LDH: salicylic acid intercalated into layered double hydroxide.

to form mixed metal oxides. The thermogravimetric (TG) profile of ZnAl-LDH is presented in Figure S1 (SI section). The TG profiles of LEV-LDH and SAL-LDH are presented in Figure 2.

For the LEV-LDH, three weight losses were observed in the thermogram (Figure 2a). The weight losses of 4.6 and 2.1% occur at temperatures of 140 and 300 °C, respectively; this may be due to the removal of surface-physiosorbed water molecules and the interlayer water of ZnAl-LDH. In addition, the weight loss of 33.7% at 440 °C corresponds to the decomposition of LEV intercalated in ZnAl-LDH. The thermogram for SAL-LDH (Figure 2b) shows that approximately 45% weight occurs between 260 and 492 °C, which may be indexed for the predominant degradation of the SAL intercalated into ZnAl-LDH. The total weight loss of LEV and SAL was less than the percentage loaded in the ZnAl-LDH, which may be because the inorganic ZnAl-LDH layers interfered with the degradation of these species.

Figure 3a shows the X-ray diffraction (XRD) patterns of ZnAl-LDH and drug-LDH. For the XRD pattern of ZnAl-LDH, diffraction peaks appeared at 2θ value of 11.59, 23.34, 31.70, 34.40, and 36.19 could be assigned to the diffraction lattice planes (003), (006), (012), (009), and (015), respectively. These diffraction peaks, which are sharp and symmetrical, are typical for hydrotalcite-like layered structure[17,31,32] and indicate the good crystallization of ZnAl-LDH. Both LEV-LDH and SAL-LDH exhibited diffraction peaks characteristic of ZnAl-LDH; however, the distance value between the d_{003} layers of LEV-LDH and SAL-LDH has clearly shifted to an angle of 2θ smaller than the pristine 2θ angle of ZnAl-LDH, indicating that LEV and SAL were successfully intercalated into the interlayers of LDH.

As seen in Figure 3a, the nanolayers of LEV-LDH and SAL-LDH have been streamlined, with a basal distance of d_{003} extended from 7.6 Å in ZnAl-LDH to 9.3 Å for LEV-LDH, and from 8.0 to 10.2 Å for SAL-LDH. The basal distance extension of d_{003} reveals a greater spatial orientation of the LEV and SAL anions in the LDH interlayer.

The functional groups of ZnAl-LDH, pure LEV, pure SAL, LEV-LDH, and SAL-LDH were identified using Fourier transform infrared spectroscopy (FTIR), as shown in Figure 3b. The presence of strong absorption peaks at 3420, 1629, and 1377 cm^{-1} in the spectrum of ZnAl-LDH were associated with the stretching mode of OH^- groups,

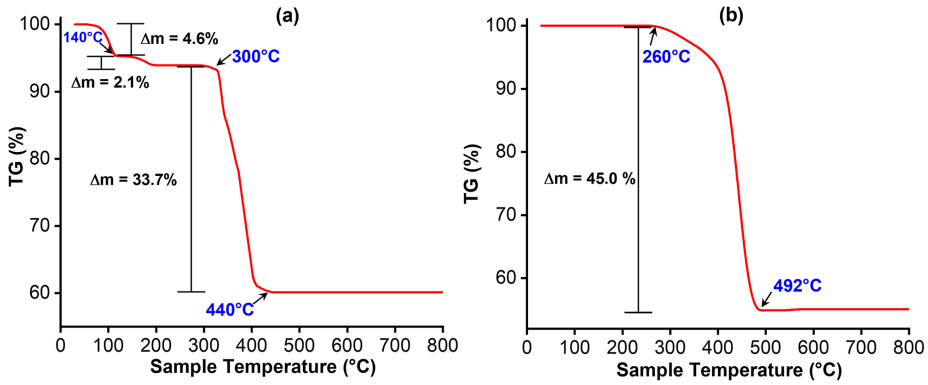

Figure 2. Thermogram for (a) LEV-LDH and (b) SAL-LDH.

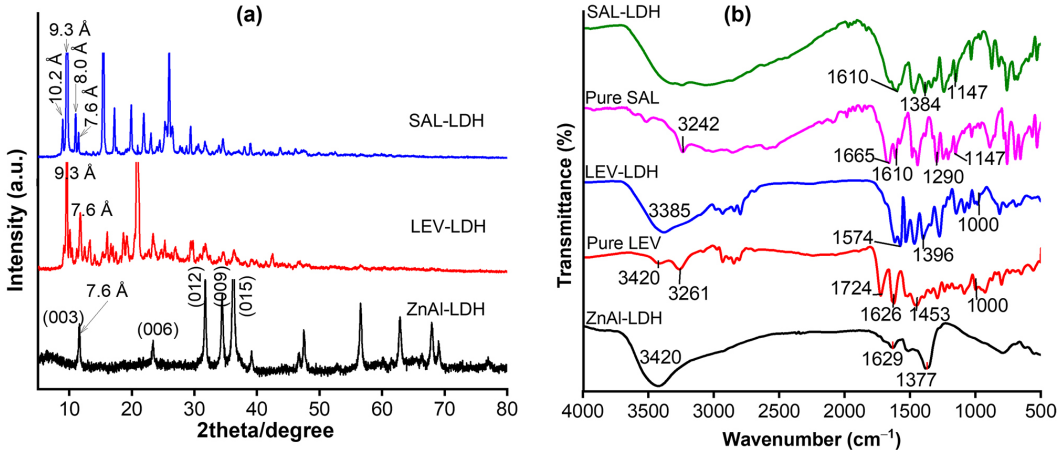

Figure 3. (a) XRD pattern and (b) FTIR (KBr) spectra of materials.

the bending mode of interlayer H_2O molecule and the NO_3^- groups in the interlayer, respectively.[17,28] For pure LEV, the strong bands observed at 1724 cm^{-1} could be related to the νC=O stretching vibrations of the carboxylic group.[33] The band at 1626 cm^{-1} corresponded to the νC=O stretching vibration of the aromatic ring[34] and the band at 1453 cm^{-1} was indexed to the symmetric stretching of the carboxylate group ($\nu_s COO^-$). In contrast to pure LEV, the absorption peak at 1724 cm^{-1} of LEV in LEV-LDH disappeared because of deprotonation of the –COOH group, resulting in the loss of C=O (–COOH) stretching. In addition, for LEV-LDH, a new vibration peak appeared at 1574 cm^{-1} and the absorption peak at 1453 cm^{-1} moved to 1396 cm^{-1}, indicating a strong interaction between LEV and the ZnAl-LDH structure. The absorption peaks at 1574 and 1396 cm^{-1} in LEV-LDH were associated to the asymmetric ($\nu_{as} COO^-$) and symmetric ($\nu_s COO^-$) stretching vibrations of the carboxylate group, respectively.[35] For pure SAL, the strong bands observed at 1665 cm^{-1} was indexed to the asymmetric stretching of the carboxylate group ($\nu_{as} COO^-$). The band at 1290 cm^{-1} could be indexed to the νC–O stretching vibrations of the carboxylic group[36] and band at 1147 cm^{-1} corresponded to the C–OH (phenolic).[36] In contrast to pure SAL, the band at 1290 cm^{-1} in SAL-LDH was almost off and that at 1665 cm^{-1} shifted to 1610 cm^{-1}, indicating that the carboxylic groups of SAL and ZnAl-LDH had a significant interaction. Two characteristic bands were observed at 1610 and 1384 cm^{-1} in SAL-LDH owing to the asymmetric and symmetric stretching of the carboxyl group, respectively, suggesting proton transfer from the –COOH group of SAL to ZnAl-LDH. The energy splitting between asymmetrical and symmetrical stretching bands ($\Delta\nu = \nu_{as} COO^- - \nu_s COO^-$) was indicative of the metal carboxylate structure and varies depending on the type of interaction between the metal and the ligand. The $\Delta\nu$ of LEV-LDH was found to be 178 cm^{-1}, indicating that the interaction between LEV and ZnAl-LDH was a bridging bidentate interaction, which means that each oxygen in the $-COO^-$ group of the intercalated LEV was covalently bonded to another Al^{3+} cation of the ZnAl-LDH lattice.[37] In case of SAL-LDH, the $\Delta\nu$ was found to be 226 cm^{-1}, indicating a monodentate interaction between SAL and ZnAl-LDH, which means that the negatively charged oxygen of the $-COO^-$ group generated a covalent bond with the metal ion.[37] This result confirms that LEV and SAL anions existed stably in the positively charged ZnAl-LDH layers owing to the bridging bidentate and monodentate interactions, respectively.

Our previous publication[28] has shown that SEM images of ZnAl-LDH had an irregular and heterogeneous morphology and was composed of agglomerated plates. Scanning electronic microscopy (SEM) image of ZnAl-LDH is presented in Figure S2 of SI section. Because of the collapse of the layered structure of ZnAl-LDH, the ZnAl-LDO particles exhibited an uneven morphology and were densely concentrated.[28] The SEM images of LEV-LDH and SAL-LDH are shown in Figure 4.

The assembly of LEV and SAL anions with the ZnAl-LDH host resulted in flat and individual plates that overlap. The formation of the plate was attributed to the interaction between LEV and SAL anions with the positively charged surface of ZnAl-LDH. Successful intercalation of LEV and SAL anions into ZnAl-LDH were due to their respective bridging bidentate and monodentate interactions. The presence of LEV in LEV-LDH and SAL in SAL-LDH were demonstrated by the energy-dispersive X-ray spectroscopy (EDX) spectrum (Figure 4). The intercalation of LEV and SAL into ZnAl-LDH resulted in an increase in the particle diameters of ZnAl-LDH from 110.2 nm[28] (Figure S2, SI section) to 202.6 nm for LEV-LDH and 208.0 nm for SAL-LDH (Figure 4).

In vitro studies of LEV-LDH and SAL-LDH

Release kinetics

Drug release depends mainly on the diffusion of drug molecules through the delivery material matrix, dissolution of the matrix, or both. The interaction between the drug carrier and the buffer solution promotes drug release at the interface between the two. Anionic LEV and SAL were conveniently located in the interlayer of ZnAl-LDH because of the positive charge density of ZnAl-LDH. In this study, LEV and SAL release assays from ZnAl-LDH carrier were conducted at 37 °C using phosphate buffer saline (PBS) at pH 7.4 and 5.8, corresponding to the pH of the wound fluid[38] and sweat of healthy skin. Physical mixtures containing 35.35% of LEV or 48.00% of SAL were prepared by grinding ZnAl-LDH with LEV or SAL in an agate mortar. The conventional release profiles of LEV and SAL from the interlayer of ZnAl-LDH carrier and the physical mixtures in PBS solution are shown in Figures 5a-5b.

The pH of the medium had little effect on the release efficiency of LEV and SAL from the interlayer of ZnAl-LDH. Therefore, release of LEV and SAL from the interlayer of ZnAl-LDH in PBS at pH 7.4 was found to be slightly slower and slightly lesser than the release in PBS at pH 5.8. The LEV and SAL in the physical mixtures released very rapidly, reaching 100% after 0.25-0.75 h at pH 7.4. In contrast, the release profiles of the LEV-LDH and SAL-LDH were significantly slower. The ZnAl-LDH released LEV and SAL in a controlled manner for up

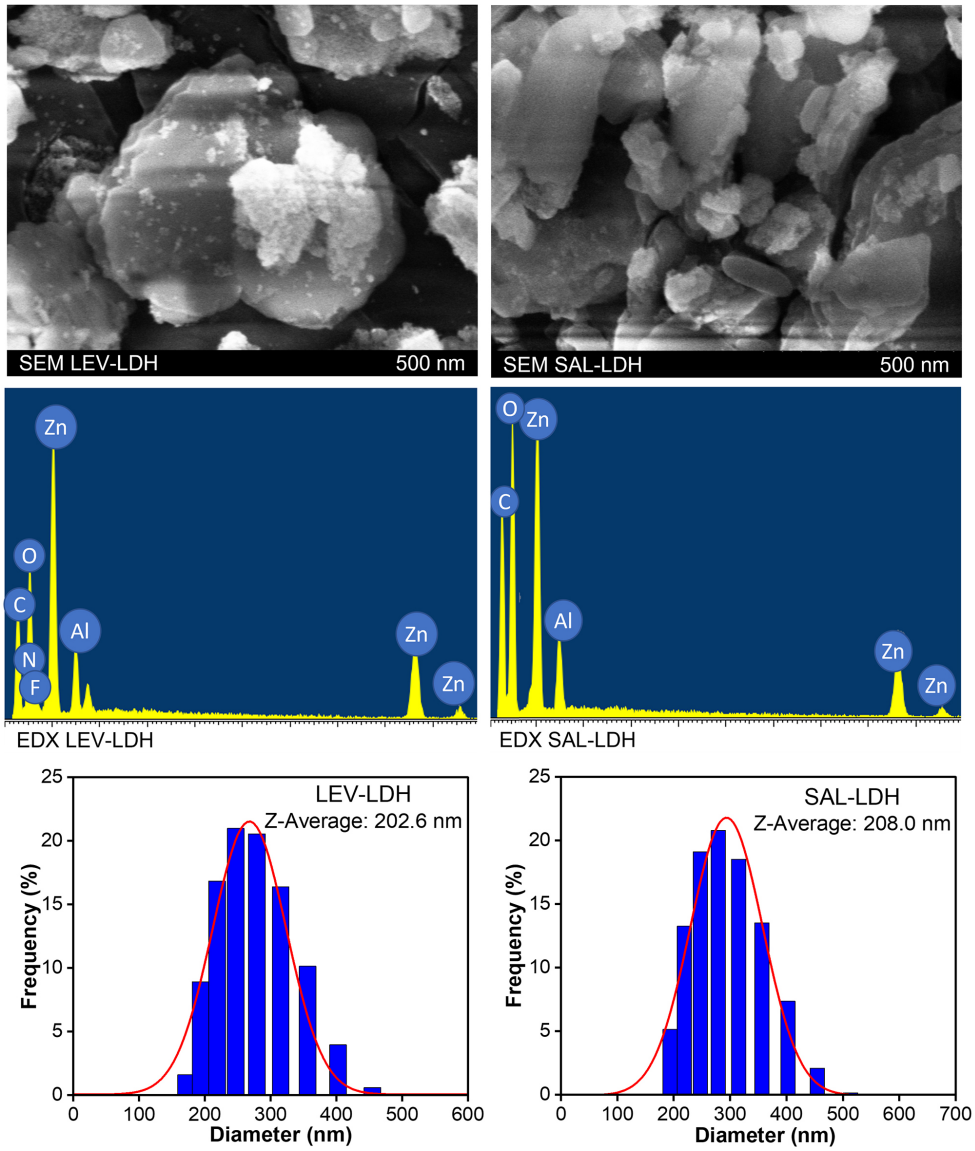

Figure 4. SEM photographs, EDX spectra and the particle size of the LEV-LDH and SAL-LDH.

to 12 h. Approximately 90.6 and 88.4% of the initially applied LEV was released after 12 h at pHs of 5.8 and 7.4, respectively. The release of SAL from the ZnAl-LDH occurred at pHs of 5.8 and 7.4, and gradually reached about 96.3 and 90.3% of the initially applied SAL within 12 h (Figure 5b).

As shown in Figures 5a-5b, the release of LEV and SAL from ZnAl-LDH included three distinct stages. The first stage (0-2 h) could be termed "burst release," i.e., rapid release through desorption of LEV and SAL surface-bound to ZnAl-LDH. The second stage (from 2-7 h) was slower than the first stage because of the ion-exchange process between OH^- and PO_4^{3-} anions in the buffer solution with LEV and SAL in the interlayer, which interacted weakly with the ZnAl-LDH layer and the migration of LEV and SAL anions from the inner region of the interlayers to the outer surface of the ZnAl-LDH.[39] The third stage (after 7 h) involved ion exchange between OH^- and PO_4^{3-} anions with LEV and SAL anions located in deeper regions of the ZnAl-LDH interlayer that diffused outward, which markedly slowed down the LEV and SAL release from ZnAl-LDH. Diffusion significantly retarded the release of LEV and SAL anions from ZnAl-LDH, respectively.[39] It is possible that approximately 10-12% of LEV and 4-10% of SAL anions could be retained in the interlayer of ZnAl-LDH. Many previous studies[11,40-42] have reported that approximately 20-23% of diclofenac and 30-40% of ciprofloxacin can be retained in ZnAl-LDH, CaAl-LDH and Fe_2O_3@MgAl-LDH. The retention of drugs in ZnAl-LDH can be explained by the exchange of LEV or SAL anions from the external ZnAl-LDH layer, which were replaced by the smaller OH^- and PO_4^{3-} anions in solution; this may have

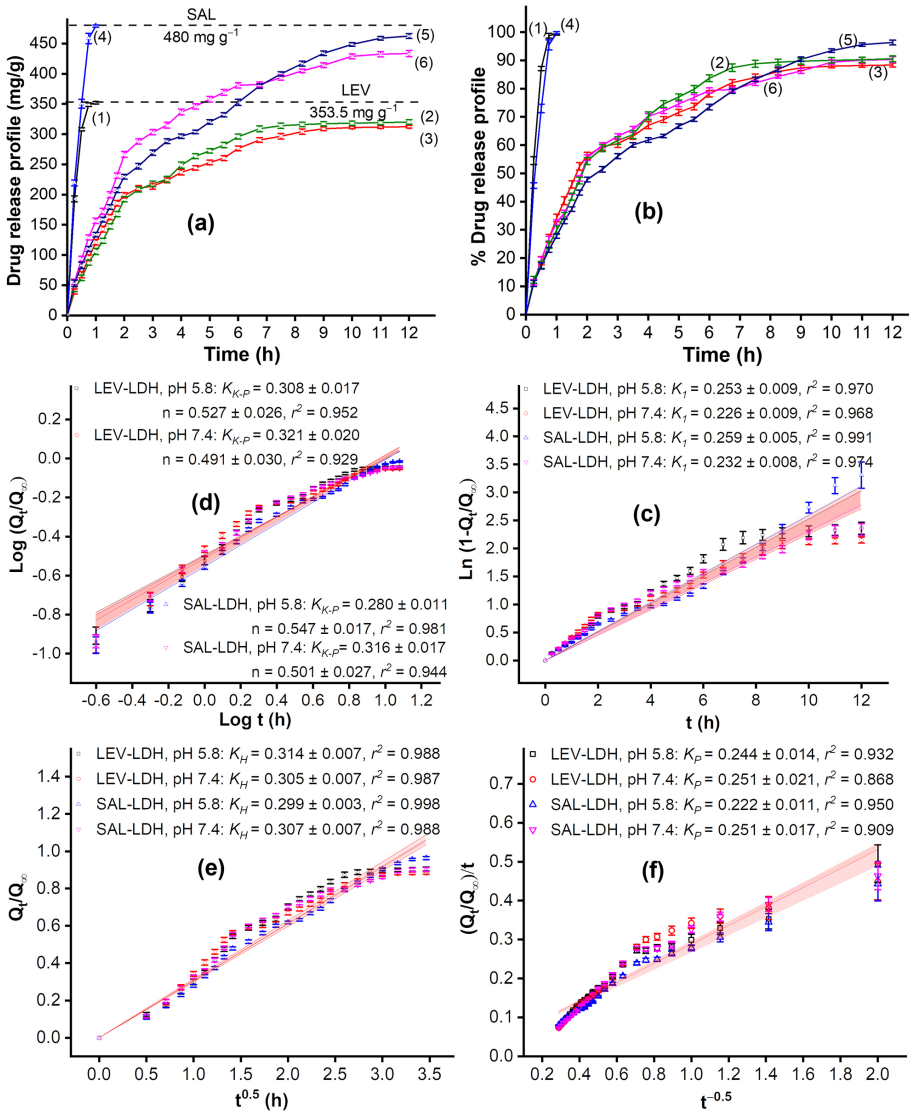

Figure 5. *In vitro* LEV and SAL release profile (a) and (b). *In vitro* LEV and SAL release kinetics (c) first order, (d) Korsmeyer-Peppas (K-P), (e) Higuchi and (f) parabolic diffusion. Error bars indicate the standard deviation of triplicates.

caused the ZnAl-LDH to recover its layered structure with smaller interlayer distances in the edge region (ca.7.6 Å), which may hinder the migration of LEV and SAL anions located deep inside the external region, leading to a certain number of drug anions that are not readily desorbed.

The mechanism by which drug release from the delivery system was mainly controlled by anion exchange and a disaggregation step,[8] diffusion and dissolution,[43,44] or combination of multiple mechanisms.[38] Various mathematical models such as first-order kinetics, Higuchi, parabolic diffusion and Korsmeyer-Peppas (K-P) were employed to analyze the kinetics of *in vitro* drug release data. The correlation coefficient (r^2), release rate constant (k), and diffusional exponent (n) were obtained and are presented in Figures 5c-5f. According to the n and r^2 values obtained from the K-P and Higuchi models, respectively, the release of LEV and SAL from the ZnAl-LDH carrier was a combination of more than one mechanism, including LEV and SAL diffusion through the interlayer of ZnAl-LDH carrier and erosion of ZnAl-LDH.[8,43,45] Diffusion plays an important role in controlling the drug-release rate, therefore the drug-release rate from the carrier is determined by the diffusion rate of the drug anions.[46] The replacement of the larger anions (LEV and SAL) at the outer edge of ZnAl-LDH by smaller anions (OH^- and PO_4^{3-}) led to a decrease in the interlayer distance and the migration of the LEV and SAL anions across the ZnAl-LDH particles became slower. Overall, the intercalation of LEV and SAL anions in ZnAl-LDH not only reduces the rate release of LEV and SAL anions, but also allows for long-term and continuous administration of LEV and SAL. The slower release rate allows an adequate

amount of the drug to be maintained for a longer period, thereby reducing the frequency of dosing while achieving the desired therapeutic effect.

Antimicrobial effectiveness and cytotoxicity

The antimicrobial study for LEV-LDH and SAL-LDH was carried out to evaluated their effectiveness against Gram-positive [(Gr (+)] bacteria (*Bacillus subtilis*) while ZnAl-LDH, pure LEV, and SAL were used as controls. For this assay, the *Bacillus subtilis* was placed in 96-well plates and treated with different concentrations of LEV-LDH, SAL-LDH or control materials. Before quantification of *Bacillus subtilis* concentration, the plates were incubated at 37 °C for 24 h. The minimum inhibitory concentration (MIC) values of pristine ZnAl-LDH for *Bacillus subtilis* was found to be 150 μg mL^{-1}, while the MICs of pure LEV and SAL for this pathogen were 200 μg mL^{-1}. LEV-LDH and SAL-LDH exhibited high efficacy, the MICs of these materials against *Bacillus subtilis* were about 100 μg mL^{-1}. As shown on Figure 6a, the zone of inhibition of LEV-LDH 100 μg mL^{-1} is larger than that of ZnAl-LDH 150 μg mL^{-1} and SAL-LDH 100 μg mL^{-1}.

The ZnAl-LDH exhibited antimicrobial properties, which can be considered as an additional advantage to the drug delivery of ZnAl-LDH. The findings of this study are completely consistent with those of previous studies. By increasing the Zn-Al molar ratio, the antimicrobial activity of pristine ZnAl-LDH could be increased.[47] In addition, the superior antibacterial effect of Zn was emphasized by Li *et al*.[48] Other work[49] found that fewer bacterial colonies grew in the presence of ZnAl-LDH (Zn:Al = 4:1) compared to other substances, and ZnAl-LDH exhibited activity against Gr (+) bacteria. LEV-LDH and SAL-LDH exhibited high efficacy against *Bacillus subtilis* due to the synergistic effects between LEV and SAL with ZnAl-LDH. This synergistic effect may be due to the ability of LEV-LDH and SAL-LDH to cross the cell membrane of the pathogen, facilitating the entry of LEV and SAL into pathogen cells, which disrupts the cell membrane and inhibits membrane reformation, leading to cell death. These observations indicate the efficacy of LEV-LDH and SAL-LDH against pathogens.

In the field of drug research and development, cytotoxicity testing has recently become a commonly used method. Cytotoxicity testing is employed to evaluate the effect of a new drug on the responses of living cells in culture, including cell survival and population growth. To determine the survival of RAW 264.7 cells, these cells were incubated with samples (ZnAl-LDH, pure SAL and SAL-LDH, pure LEV and LEV-LDH) at 10, 30, and 100 μg mL^{-1} for 24 h. The 3-(4,5-dimethylthiazol-2-yl)-2,5-diphenyltetrazolium bromide (MTT) dye reduction assay was employed to measure the cell survival.[50] Figure 6b shows the survival of RAW 264.7 cells and suppression of

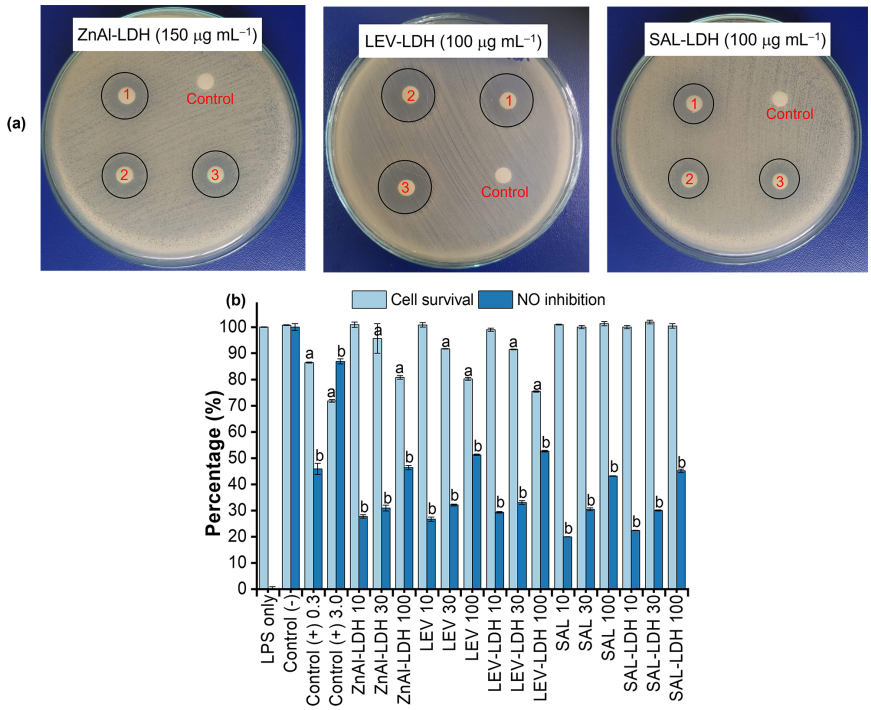

Figure 6. (a) Inhibition zone (1,2,3) corresponds to ZnAl-LDH 150 μg mL^{-1} or LEV-LDH and SAL-LDH 100 μg mL^{-1}; (b) effects of LEV-LDH and SAL-LDH on RAW 264.7 cells survival and suppression of NO production (mean ± standard deviation, n = 3). Cardamonin (0.3 and 3 μM) is used as control (+). Letters a and b indicate that cell survival and NO inhibition were significantly different from control (–) at the 0.05 level (least significant difference (LSD) test).

NO production by RAW 264.7 cells after treatment with the samples. As shown in Figure 6b, more than 80% of RAW 264.7 macrophages survived after treatment with ZnAl-LDH concentrations ranging from 10 to 100 μg mL^{-1}, which confirms that ZnAl-LDH has negligible negative effect on RAW 264.7 macrophages. The non-toxicity of ZnAl-LDH particles is believed to be an advantage for their use in human drug delivery. Approximately 100.83 ± 0.84 and 91.74 ± 0.11% of RAW 264.7 cells survived after treatment with pure LEV at concentrations of 10 and 30 μg mL^{-1}, respectively (Figure 6b). However, the RAW 264.7 cell survival decreased to 80.25 ± 0.51% with increasing concentration of pure LEV up to 100 μg mL^{-1}. After treatment with LEV-LDH at concentrations of 10 and 30 μg mL^{-1}, the survivals of RAW 264.7 cells were found to be approximately 99.01 ± 0.58 and 91.48 ± 0.14%, respectively. Cell growth was decreased with increasing LEV-LDH concentration; approximately 75.40 ± 0.26% of RAW 264.7 cells survived when the LEV-LDH concentration was increased to 100 μg mL^{-1}. This demonstrated that LEV-LDH at high concentrations could be toxic to RAW 264.7 cells. However, at the same concentrations of pure SAL and SAL-LDH, the viability of RAW 264.7 macrophages were higher than 100% relative to cardamonin as positive control ($p < 0.05$). Previous study[51] have reported that HepG2 cell growth is significantly inhibited owing to the simultaneous intercalation of tamoxifen and hippuric acid into zinc layer hydroxides. Because of its intercalation into LDH, folic acid is protected from degradation and favorably permeates HeLa cells, resulting in the suppression of cell survival.[52] The interaction between ciprofloxacin and zinc hydroxide led to sustained release of ciprofloxacin anions, resulting in increased cytotoxic effects on A549 cells.[53]

In addition, ZnAl-LDH, pure LEV, pure SAL, LEV-LDH, and SAL-LDH were investigated for their ability to alter NO generation in lipopolysaccharide (LPS)-stimulated RAW 264.7 macrophages. In order to perform this experiment, LPS treatment was used to stimulate increased intracellular nitrite accumulation. RAW 264.7 macrophages were simultaneous treated with 2 μL LPS (0.1 mg mL^{-1}) and ZnAl-LDH, pure LEV, pure SAL, LEV-LDH or SAL-LDH at different concentration. The concentration of nitrite in the culture media was measured to determine the NO yield. As seen in Figure 6b, LPS-stimulated RAW 264.7 macrophages treated with cardamonin at concentrations of 0.3 and 3.0 μM inhibited NO formation by about 45.85 ± 2.12 and 86.93 ± 0.96%, respectively. The significant reduction in NO generation for LPS-stimulated RAW 264.7 macrophages treated with 3.0 μM cardamonin may be related to cell damage (with a viability of about 71.8%). In general, the decrease in NO levels was pronounced. A decrease in NO generation was also observed in LPS-stimulated RAW 264.7 cells after treatment with ZnAl-LDH, LEV-LDH and SAL-LDH. Compared with control cells, LPS-stimulated RAW 264.7 cells treated with pristine ZnAl-LDH at concentrations of 10 and 30 μg mL^{-1} induced a reduction in NO of 27.73 ± 0.65 and 30.91 ± 1.12%, respectively. For LPS-stimulated RAW 264.7 macrophages treated with LEV-LDH at concentrations of 10 and 30 μg mL^{-1}, a reduction in NO was observed of approximately 29.3 ± 0.28 and 33.02 ± 0.73%, respectively. For LPS-stimulated RAW 264.7 macrophages treated with SAL-LDH at concentrations of 10 and 30 μg mL^{-1} induced a reduction in NO of 22.38 ± 0.03 and 30.01 ± 0.18%, respectively. For LPS-stimulated RAW 264.7 macrophages treated with either ZnAl-LDH or SAL-LDH or LEV-LDH at high concentration induced a significant reduction in NO generation. The ZnAl-LDH, SAL-LDH and LEV-LDH at high concentrations (100 μg mL^{-1}) induced a reduction in NO of 46.36 ±0.82, 45.15 ± 0.67, and 52.62 ± 0.31% respectively. Significant inhibitory effects on the NO release by pristine ZnAl-LDH and LEV-LDH were observed at high concentrations, which may be associated with cell damage (with viabilities of 80.8 ± 0.73 and 75.40 ± 0.26%, respectively). The inhibitory concentration of NO formation (IC_{50}) by ZnAl-LDH, SAL-LDH and LEV-LDH were found to be greater than 100 μg mL^{-1}.

Conclusions

The three-level-three-factor FC-CCD in combination with RSM was used to investigate the effect of parameters on intercalation of LEV and SAL into the structure of ZnAl-LDH. The 3D response surface plots and quadratic equations helped to predict and validate the values of independent variables for the optimization with desired intercalation efficiency. The successful intercalation of LEV and SAL into the structure of ZnAl-LDH extended the basal spacing of ZnAl-LDH. The basal spacing of ZnAl-LDH was extended from 7.6 Å up to 9.3 Å for LEV intercalation and up to 8.0-10.2 Å for SAL intercalation. Owing to the reciprocal interaction between the LEV and SAL anions with the lattice of ZnAl-LDH, as well as the slow diffusion of LEV and SAL anions from deep inside of the interlayer of ZnAl-LDH to the outside, the release rate of LEV and SAL from the ZnAl-LDH carrier is relatively slow. From the results of the antimicrobial assay of LEV-LDH and SAL-LDH, as well as the suppression of NO production and survival of LPS-stimulated RAW 264.7 macrophages after treatment with LEV-LDH and SAL-LDH, it can

be conjectured that a synergistic effect between LEV and SAL with ZnAl-LDH occurred. Overall, ZnAl-LDH appears to be a sustainable drug delivery system that can maintain dosage during treatment thereby increasing the effectiveness of antibiotics and anti-inflammatory drugs and significantly reducing drug side effects. These results provide a solid foundation for further research on a biocompatible ZnAl-LDH carrier-based drug delivery system.

Supplementary Information

Supplementary data (synthesis and characterization of the ZnAl-LDH, LEV-LDH or SAL-LDH, *in vitro* release kinetics study, antimicrobial activity assay, cytotoxicity assays; thermogram for ZnAl-LDH and SEM images of the ZnAl-LDH and ZnAl-LDO, EDX spectra and the particle size of the ZnAl-LDH) are available free of charge at http://jbcs.sbq.org.br as PDF file.

Author Contributions

NTTV was responsible for conceptualization, data curation, writing the original draft; DNNK for validation, data curation; LHK for validation, data curation; NTP for validation, data curation; NQT for validation, data curation; LHT for validation, data curation; NTHN for validation, data curation; DTMP for validation, data curation; NTKP for conceptualization, visualization, writing the original draft, writing review and editing.

References

1. Rives, V.; Del Arco, M.; Martín, C.; *J. Controlled Release* **2013**, *169*, 28. [Crossref]
2. Ladewig, K.; Niebert, M.; Xu, Z. P.; Gray, P. P.; Lu, G. Q. M.; *Biomaterials* **2010**, *31*, 1821. [Crossref]
3. Ladewig, K.; Niebert, M.; Xu, Z. P.; Gray, P. P.; Lu, G. Q.; *Appl. Clay Sci.* **2010**, *48*, 280. [Crossref]
4. Oh, J.-M.; Choi, S.-J.; Kim, S. T.; Choy, J. H.; *Bioconjugate Chem.* **2006**, *176*, 1411. [Crossref]
5. Oh, J. M.; Choi, S. J.; Lee, G. E.; Kim, J. E.; Choy, J. H.; *Chem. Asian. J.* **2009**, *4*, 67. [Crossref]
6. Wang, Q.; O'Hare, D.; *Chem. Rev.* **2012**, *112*, 4124. [Crossref]
7. Oh, J.-M.; Biswick, T. T.; Choy, J.-H.; *J. Mater. Chem.* **2009**, *19*, 2553. [Crossref]
8. Panda, H. S.; Srivastava, R.; Bahadur, D.; *J. Phys. Chem. B* **2009**, *113*, 15090. [Crossref]
9. Gordijo, C. R.; Barbosa, C. A. S.; Ferreira, A. M. C.; Constantino, V. R. L.; Silva, D. O.; *J. Pharm. Sci.* **2005**, *94*, 1135. [Crossref]
10. Luengo, C. V.; Crescitelli, M. C.; Lopez, N. A.; Avena, M. J.; *J. Pharm. Sci.* **2021**, *110*, 1779. [Crossref]
11. Yousefi, V.; Tarhriz, V.; Eyvazi, S.; Dilmaghani, A.; *J. Nanobiotechnol.* **2020**, *18*, 155. [Crossref]
12. Mansouri, E.; Tarhriz, V.; Yousefi, V.; Dilmaghani, A.; *Adsorption* **2020**, *26*, 835. [Crossref]
13. Cherif, N. F.; Constantino, V. R. L.; Hamdaoui, O.; Leroux, F.; Taviot-Guého, C.; *New J. Chem.* **2020**, *44*, 10076. [Crossref]
14. Choi, G.; Kim, T.-H.; Oh, J.-M.; Choy, J.-H.; *Coord. Chem. Rev.* **2018**, *359*, 32. [Crossref]
15. Kim, T.-H.; Lee, G.-J.; Kang, J.-H.; Kim, H.-J.; Kim, T.-i.; Oh, J.-M.; *Biomed Res. Int.* **2014**, *2014*, 193401. [Crossref]
16. Rui, L.; *Compr. Physiol.* **2014**, *4*, 177. [Crossref]
17. Zhang, X. Q.; Zeng, M. G.; Li, S. P.; Li, X. D.; *Colloids Surf., B* **2014**, *117*, 98. [Crossref]
18. Tang, L.-P.; Cheng, H.-M.; Cui, S.-M.; Wang, X.-R.; Song, L.-Y.; Zhou, W.; Li, S.-J.; *Colloids Surf., B* **2018**, *165*, 111. [Crossref]
19. Perioli, L.; Posati, T.; Nocchetti, M.; Bellezza, F.; Costantino, U.; Cipiciani, A.; *Appl. Clay Sci.* **2011**, *53*, 374. [Crossref]
20. Frunza, M.; Lisa, G.; Popa, M. I.; Miron, N. D.; Nistor, D. I.; *J. Therm. Anal. Calorim.* **2008**, *93*, 373. [Crossref]
21. Ryu, S.-J.; Jung, H.; Oh, J.-M.; Lee, J.-K.; Choy, J.-H.; *J. Phys. Chem. Solids* **2010**, *71*, 685. [Crossref]
22. San Román, M. S.; Holgado, M. J.; Salinas, B.; Rives, V.; *Appl. Clay Sci.* **2013**, *71*, 1. [Crossref]
23. Yasin, Y.; Ismail, N. M.; *J. Med. Sci.* **2013**, *13*, 453. [Crossref]
24. Barahuie, F.; Hussein, M. Z.; Arulselvan, P.; Fakurazi, S.; Zainal, Z.; *J. Solid State Chem.* **2014**, *217*, 31. [Crossref]
25. Yasaei, M.; Khakbiz, M.; Ghasemi, E.; Zamanian, A.; *Appl. Surf. Sci.* **2019**, *467-468*, 782. [Crossref]
26. Chakraborty, M.; Dasgupta, S.; Soundrapandian, C.; Chakraborty, J.; Ghosh, S.; Mitra, M. K.; Basu, D.; *J. Solid State Chem.* **2011**, *184*, 2439. [Crossref]
27. Yin, S.; Chen, Y.; Li, C.; Qiu, X.; Zhang, Y.; Li, Y.; *J. Iran. Chem. Soc.* **2022**, *19*, 3043. [Crossref]
28. Vy, N. T. T.; Khanh, D. N. N.; Khanh, P. D.; Phat, N. T.; Anh, N. T.; Nguyen, N. L.; Anh, T. N. L.; Vy, N. N.; Dan, L. T. M.; Phuong, N. T. K.; *J. Cluster Sci.* **2023**, *34*, 2619. [Crossref]
29. *MODDE*, version 5.0; Umetrics AB; Umea, Sweden, 1999.
30. *Design-Expert*, version 13.0.5.0; StatEase Inc.; Minneapolis, USA, 2021.
31. Busetto, C.; Del-Piero, G.; Manara, G.; Trifirò, F.; Vaccari, A.; *J. Catal.* **1984**, *85*, 260. [Crossref]
32. Li, A.; Deng, H.; Ye, C.; Jiang, Y.; *ACS Omega* **2020**, *5*, 15152. [Crossref]
33. Mouzam, M. I.; Dehghan, M. H. G.; Asif, S.; Sahuji, T.; Chudiwal, P.; *Saudi Pharm. J.* **2011**, *19*, 85. [Crossref]
34. Munir, A.; Sirajuddin, M.; Zubair, M.; Haider, A.; Tirmizi, S. A.; Ali, S.; Khan, H.; Ullah, K.; Aziz, I.; *Russ. J. Gen. Chem.* **2017**, *87*, 2380. [Crossref]
35. Nugrahani, I.; Laksana, A. N.; Uekusa, H.; Oyama, H.; *Molecules* **2022**, *27*, 2166. [Crossref]

36. Guan, X.-h.; Chen, G.-h.; Shang, C.; *J. Environ. Sci.* **2007**, *19*, 438. [Crossref]
37. Barnakov, Y. A.; Idehenre, I. U.; Basun, S. A.; Tyson, T. A.; Evans, D. R.; *Nanoscale Adv.* **2019**, *1*, 664. [Crossref]
38. Costa, P.; Sousa Lobo, J. M.; *Eur. J. Pharm. Sci.* **2001**, *13*, 123. [Crossref]
39. Zobir bin Hussein, M.; Hj Yahaya, A.; Zainal, Z.; Hee Kian, L.; *Sci. Technol. Adv. Mater.* **2005**, *6*, 956. [Crossref]
40. Joy, M.; Iyengar, S. J.; Chakraborty, J.; Ghosh, S.; *Front. Mater. Sci.* **2017**, *11*, 395. [Crossref]
41. Ma, Y.; Zhang, S.; Wang, Y.; Jiang, Z.; Fu, N.; Yang, Z.; Mao, Y.; *Nano* **2020**, *15*, 2050028. [Crossref]
42. Jadam, M. L.; Syed Mohamad, S. A.; Zaki, H. M.; Jubri, Z.; Sarijo, S. H.; *J. Drug Delivery Sci. Technol.* **2021**, *62*, 102314. [Crossref]
43. Higuchi, T.; *J. Pharm. Sci.* **1963**, *52*, 1145. [Crossref]
44. DeLeon, V. H.; Nguyen, T. D.; Nar, M.; D'Souza, N. A.; Golden, T. D.; *Mater. Chem. Phys.* **2012**, *132*, 409. [Crossref]
45. Siepmann, J.; Peppas, N. A.; *Adv. Drug Delivery Rev.* **2001**, *48*, 139. [Crossref]
46. Wei, M.; Pu, M.; Guo, J.; Han, J.; Li, F.; He, J.; Evans, D. G.; Duan, X.; *Chem. Mater.* **2008**, *20*, 5169. [Crossref]
47. Lobo-Sánchez, M.; Nájera-Meléndez, G.; Luna, G.; Segura-Pérez, V.; Rivera, J. A.; Fetter, G.; *Appl. Clay Sci.* **2018**, *153*, 61. [Crossref]
48. Li, M.; Sultanbawa, Y.; Xu, Z. P.; Gu, W.; Chen, W.; Liu, J.; Qian, G.; *Colloids Surf., B* **2019**, *174*, 435. [Crossref]
49. Cheng, H.-M.; Gao, X.-W.; Zhang, K.; Wang, X.-R.; Zhou, W.; Li, S.-J.; Cao, X.-L.; Yan, D.-P.; *New J. Chem.* **2019**, *43*, 19408. [Crossref]
50. Choi, S.-J.; Choi, G.-E.; Oh, J.-M.; Oh, Y.-J.; Park, M.-C.; Choy, J.-H.; *J. Mater. Chem.* **2010**, *20*, 9463. [Crossref]
51. Hussein Al Ali, S. H.; Al-Qubaisi, M.; Hussein, M. Z.; Zainal, Z.; Hakim, M. N.; *Int. J. Nanomed.* **2011**, *6*, 3099. [Crossref]
52. Li, Y.; Liu, D.; Ai, H.; Chang, Q.; Liu, D.; Xia, Y.; Liu, S.; Peng, N.; Xi, Z.; Yang, X.; *Nanotechnology* **2010**, *21*, 105101. [Crossref]
53. Abdul-Latip, A. F.; Hussein, M. Z.; Stanslas, J.; Wong, C. C.; Adnan, R.; *Chem. Cent. J.* **2013**, *7*, 119. [Crossref]

Submitted: May 10, 2023
Published online: November 9, 2023